Comparative study on two-constant-amplitude input shapers to maneuver flexible satellite in small structural deflection

Setyamartana PARMAN*,[1], Affiani MACHMUDAH[2,3], Vu Trieu MINH[4]

*Corresponding author
*,[1]Fakulti Kejuruteraan Mekanikal dan Pembuatan,
Universiti Teknikal Malaysia Melaka, Durian Tunggal, Melaka, Malaysia,
setyamartana@utem.edu.my
[2]Faculty of Advanced Technology and Multidiscipline,
Kampus C Jalan Mulyorejo, Universitas Airlangga, Surabaya 60115, Indonesia,
affiani.machmudah@ftmm.unair.ac.id
[3]Research Center for Hydrodynamics Technology,
National Research and Innovation Agency (BRIN),
Jl. Hidro Dinamika, Keputih, Sukolilo, Surabaya 60112, Indonesia
[4]Institute for Nanomaterials, Advanced Technologies and Innovation,
Technical University of Liberec,
461 17 Liberec, Czech Republic,
vutrieuminh@gmail.com

DOI: 10.13111/2066-8201.2022.14.3.5

Received: 22 June 2021/ Accepted: 22 August 2022/ Published: September 2022

Abstract: *The satellite attitude maneuver using thrusters is studied in this paper. The satellite consists of a rigid main body and two symmetrical solar panels that are so large that their flexibility cannot be neglected. The finite element method is used to discretize the elastic motion of the solar panels. The solar panels are modeled as a set of rectangular plate elements and only out-of-plane displacement is taken into account. The satellite is controlled by a thruster in its main body, while there are no other control inputs on the solar panels. For the attitude maneuver, the roll, pitch and yaw torques generated by the on-off thruster are used and here can produce two different constant amplitudes. Then two types of fuel-efficient input shaping are formulated and applied to perform satellite attitude correction. The first type of input LHHL is preceded by the use of a small amplitude torque followed by a large amplitude one, while the sequence of torque applied to the second type of input HLLH is the opposite of the first input. The two types of inputs are applied separately to the same satellite. They managed to dampen the residual vibrations after reaching the desired attitude, but in achieving this condition the solar panels experienced considerable deflection during the transient response. Due to this, the effectiveness of the shaped inputs for maneuvering the satellites at small structural deflections of the solar panels during their transient responses is compared. The simulation results show that the use of the LHHL input shaper can minimize the structural deflection that occurs in the transient response during the satellite attitude maneuvering process.*

Key Words: *input shaper, flexible satellite, attitude maneuver, transient response, finite element, fuel-efficient*

1. INTRODUCTION

Communication satellites, which are usually placed in geostationary orbits, have grown in size in recent years. The Intelsat 30, which uses the LS-1300 satellite platform, introduced in the late 1980s, has a wingspan of 32.4 meters for the solar panels [1]. The Boeing 702MP satellite platform, introduced in 2009 has a wing span of solar panels in the range of 36.9-38.1 meters [2]. The Wideband Global Satcom WGS-9 launched in 2017 is a satellite constellation system that has individual satellites on a Boeing BSS-702HP satellite platform using solar boards with a wingspan of 41 meters [3].

From the three examples of satellites, it can be predicted that in order to produce energy with greater power, the satellite's solar panels will increase in size and length in the future. Due to the limited mass at launch, the satellite is designed using lightweight materials. With the increase in the size of the satellite but coupled with the use of lightweight materials, the satellite can no longer be considered a rigid system because the flexibility of the satellite can no longer be ignored.

Geostationary communication satellites require a certain precision in pointing to the earth. To maintain orientation, satellites often require attitude correction during their lifetime in orbit. Attitude maneuvers of rigid satellites can be carried out easily without causing structural vibrations and attitude oscillations.

However, attitude maneuvers of flexible satellites can cause vibration problems after steady state, especially when they are performed using on-off thrusters. To overcome this problem, the method of shaping the input generated by the thruster has been demonstrated by Parman [4, 5, 6, 7, 8, 9] and other researchers [10, 11, 12, 13, 14, 15, 16, 17]. Their study investigated the shaping of inputs with constant amplitude, in either the fuel-efficient or time-optimal type. By using the shaping input, they managed to dampen the structural vibrations and attitude oscillations at steady state.

However, it is found that the elastic deflection of the solar panels is still quite large during the transient conditions. Of course, this large enough deflection is quite worrying because it might cause the structure of the solar panels to break.

Several works investigated the elastic deflection of a driven system using input shaping during transient responses [18, 19, 20, 21, 22, 23]. Robertson [24] formulated an analytical approach in the input shaping constraint to overcome the large transient deflections during the maneuver of the spring-mass system.

For the type of system that has a single vibrating mode as studied, the analytical formulation of the input constraint can be easily defined. However, when the system has more flexible modes, the analytical equations for limiting the deflection of the flexible members become very complex and impossible to formulate. Computational simulation then becomes the solution, such as research conducted by Parman [25, 26] which uses a finite element model for flexible satellites and is controlled by a constant amplitude input shaper. In this paper, computer simulations of flexible satellite's attitude maneuvers are presented. The satellite under review consists of a main body and two large, symmetrical flexible solar panels. Maneuvering is controlled by the torque generated by the thruster system, where the torque generated can have two different amplitudes.

Two types of fuel-efficient input shapers are formulated in this paper and applied to control the satellite in the simulation. The satellite in the finite element model that has been developed by Parman [4, 5, 8] with a non-zero offset angle of the solar panel is used for simulation. The effectiveness of the input shaper to have a small deflection of the solar panels during transient conditions will finally be concluded.

2. SATELLITE WITH TWO FLEXIBLE SYMMETRICAL SOLAR PANELS

2.1 Finite element modelling

The flexible satellite model investigated in this work is the same as the model used in Ref. [4, 5, 8]. The satellite has a rigid main body and two solar panels which are symmetrical, light, large and long. Therefore, solar panels are flexible. The finite element model of the satellite is shown in Fig. 1.

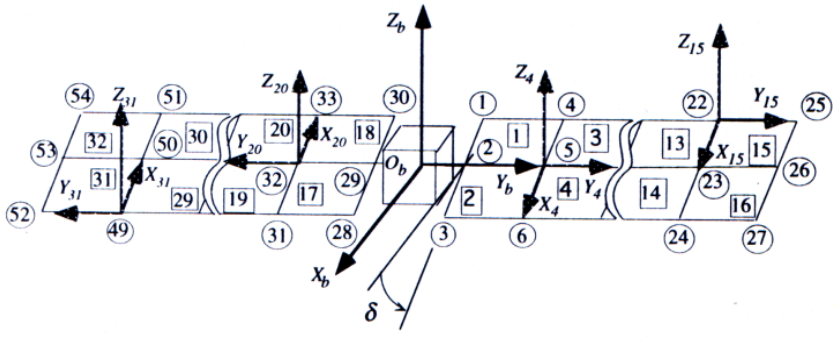

Fig. 1 – Finite element model of satellite [4]

For finite element modeling, each solar panel is divided into sixteen rectangular plate elements and only out-of-plane deflection is taken into account. Then, these rectangular plate elements are considered as isotropic materials. The $OX_bY_bZ_b$ reference frame is attached to the main body in the middle of the line connecting the rotating axis of the solar panel. Under normal operating conditions without disturbance, the X_b axis coincides with the satellite's velocity line which is tangent to its orbital trajectory, the Z_b axis points towards the earth, while the Y_b axis coincides with the rotating axis of the solar panel and completes the reference frame system by following the right hand rule. The solar panel elements in the positive Y_b axis direction are numbered 1 through 16, while the elements in the other solar panel are numbered 17 to 32. A local reference frame is attached to each plate element at the undeform state. This frame of reference serves to express out-of-plane deflections from points in the element. The solar panel nodal points in the positive Y_b axis are marked with numbers ranging from 1 to 27, while numbers 28 to 54 are used to notify the nodal points of the other side of the solar panel.

In the finite element method, the number of elements needed to model an object is as much as possible. The more the number of elements, the better the results that will be obtained because the model will be closer to the original object. However, in the case of these solar panels, the actual object is not made of a single isotropic material. Solar panels are composed of several layers of different materials [27] accompanied by a reinforcing frame, for example from aluminum. However, in terms of its flexibility in deflecting out-of-plane in this paper, it is considered an isotropic material. Therefore the selection of the number of rectangular plate elements of the solar panel is not too critical. The number of elements does not need to be too much, the important thing is that it can represent a number of out-of-plane vibration modes of the solar panel.

2.2 Satellite attitude

The satellite attitude can be expressed in various ways, for example in Euler parameters, Euler angles or Bryant's angles. For attitude maneuvers involving large changes in attitude angles, researchers usually use Euler parameters, for example, as done by Robinett et al. [28], while for small changes in attitude angles, researchers prefer to use Euler or Bryant's angles. The

attitude of the satellite in this paper is stated in Bryant's angles: roll ϕ, pitch θ and yaw ψ angles with respect to the observation reference frame F_o, while the orbital reference frame was chosen as the reference frame of observation. The definition of the Bryant angle is shown in Fig. 2.

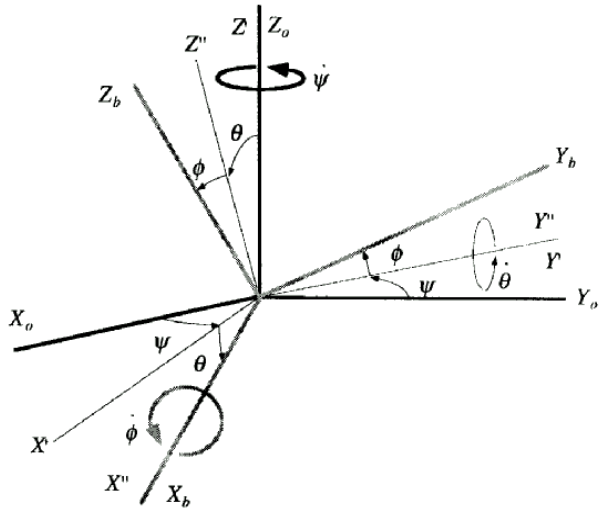

Fig. 2 – Bryant's angles for rotations from F_o to F_b

2.3 Equation of motion

The satellite's equation of motion follows the derivation of Parman et al [4, 5, 8], which can be expressed in the following linear equation:

$$\begin{bmatrix} m\mathbf{U}_3 & \mathbf{Q} & \mathbf{W} \\ \mathbf{Q}^T & \mathbf{I} & \mathbf{A} \\ \mathbf{W}^T & \mathbf{A}^T & \mathbf{M} \end{bmatrix} \begin{Bmatrix} \ddot{\boldsymbol{r}} \\ \ddot{\Theta} \\ \ddot{\boldsymbol{d}} \end{Bmatrix} + \begin{bmatrix} \mathbf{0}_{3\times3} & \mathbf{Q}\tilde{\omega}_o & \mathbf{0}_{3\times f} \\ \mathbf{0}_{3\times3} & \mathbf{I}\tilde{\omega}_o & \mathbf{0}_{3\times f} \\ \mathbf{0}_{f\times3} & \mathbf{A}^T\tilde{\omega}_o & \mathbf{D}_{f\times f} \end{bmatrix} \begin{Bmatrix} \dot{\boldsymbol{r}} \\ \dot{\Theta} \\ \dot{\boldsymbol{d}} \end{Bmatrix} + \begin{bmatrix} \mathbf{0}_{3\times3} & \mathbf{0}_{3\times3} & \mathbf{0}_{3\times f} \\ \mathbf{0}_{3\times3} & \mathbf{0}_{3\times3} & \mathbf{0}_{3\times f} \\ \mathbf{0}_{f\times3} & \mathbf{0}_{f\times3} & \mathbf{K} \end{bmatrix} \begin{Bmatrix} \boldsymbol{r} \\ \Theta \\ \boldsymbol{d} \end{Bmatrix} = \begin{Bmatrix} \boldsymbol{F}_b \\ \boldsymbol{T}_b \\ \boldsymbol{F}_a \end{Bmatrix} \tag{1}$$

In Equation (1) m is the total mass of satellite, **A** is the coupling matrix for the rotational displacements of the main body and the elastic displacements of the solar panels, and **W** is the coupling matrix for the translational displacements of the main body and the elastic displacements of solar panels.

The rigid main body coupling matrix for the translation and rotation of displacements is symbolized by **Q**, while the satellite inertia and solar panel's mass matrices are identified by **I** and **M**, respectively.

The **K** is designated for the matrix of solar panel's stiffness. The damping property of solar panels in the matrix form is represented in **D**.

The matrix $\tilde{\boldsymbol{\omega}}_o$ represents the skew symmetric matrix of the satellite orbital velocity ω_o. The rigid main body's translational and rotational displacements are expressed in vectors $\boldsymbol{r}$ and $\boldsymbol{\Theta}$, respectively. Here $\boldsymbol{\Theta}$ is stated in the Bryant's angles vector. The vector $\boldsymbol{d}$ is the elastic out-of-plane displacements of the satellite's solar panels.

The vectors $\boldsymbol{F}_b$ and $\boldsymbol{T}_b$ state external forces and torques those are working on the rigid main body, respectively.

The external forces and torques working on the solar panels form the vector $\boldsymbol{F}_a$. The total degrees of freedom of the flexible solar panels is noted in f. In fact, flexible solar panels have attenuation properties even though they are quite small.

The most serious condition is when this damping property is absent. In this research article, flexible solar panels are considered to have very small dissipation properties that can be ignored. This is to show that the control method used here is capable of overcoming the most severe conditions. So, the matrix **D** in Equation (1) is equal to **0**.

3. FASTEST ATTITUDE MANEUVER

The satellite studied here does not have control inputs on the solar panels. The control input for attitude maneuvers is only in the form of torque generated by the on-off reaction thruster in constant amplitude in the main body.

Based on Newton's second law of rotational motion, the angular acceleration of the attitude of the satellite as a rigid body motion can be expressed as:

$$\begin{Bmatrix} \ddot{\phi} \\ \ddot{\theta} \\ \ddot{\psi} \end{Bmatrix} = \begin{bmatrix} I_{xx} & I_{xy} & I_{xz} \\ I_{xy} & I_{yy} & I_{yz} \\ I_{xz} & I_{yz} & I_{zz} \end{bmatrix}^{-1} \begin{Bmatrix} T_{b_x} \\ T_{b_y} \\ T_{b_z} \end{Bmatrix} \tag{2}$$

where I_{xx}, I_{yy}, I_{zz}, I_{xy}, I_{xz}, and I_{yz} are components of the whole satellite's inertia matrix I, and T_{bx}, T_{by}, and T_{bz} are components of the torque input vector $\mathbf{T}_b$ on the rigid main body in Equation (1). For small angular displacements and angular velocities, a desired angular velocity can be determined by integrating Equation (2) with respect to time,

$$\begin{Bmatrix} \dot{\phi}_d \\ \dot{\theta}_d \\ \dot{\psi}_d \end{Bmatrix} = \int \begin{bmatrix} I_{xx} & I_{xy} & I_{xz} \\ I_{xy} & I_{yy} & I_{yz} \\ I_{xz} & I_{yz} & I_{zz} \end{bmatrix}^{-1} \begin{Bmatrix} T_{b_x} \\ T_{b_y} \\ T_{b_z} \end{Bmatrix} dt \tag{3}$$

Finally, if Equation (3) is integrated, a desired attitude angle displacement can be produced,

$$\begin{Bmatrix} \phi_d \\ \theta_d \\ \psi_d \end{Bmatrix} = \int \int \begin{bmatrix} I_{xx} & I_{xy} & I_{xz} \\ I_{xy} & I_{yy} & I_{yz} \\ I_{xz} & I_{yz} & I_{zz} \end{bmatrix}^{-1} \begin{Bmatrix} T_{b_x} \\ T_{b_y} \\ T_{b_z} \end{Bmatrix} dt\, dt \tag{4}$$

In simulations, the satellite of Parman [25] is used for this study. The main body of the satellite is supposed to be consisted of six lumped masses at certain location from the center of the reference frame of the rigid main body O_b. The values and locations of the lumped masses are tabulated in Table 1. Table 2 lists the solar panel parameters of the satellites used in the computer simulation. For the configuration under consideration the center of the main rigid body fixed reference frame coincides with the center of mass of the whole satellite in undeform state. The values of I_{xx}, I_{yy}, I_{zz}, I_{xy}, I_{yz} and I_{xz} are 17,731 kg·m^2, 2,580 kg·m^2, 15,557kg·m^2, 0 and 43 kg·m^2, respectively.

Table 1 – Lumped masses in the main body

Mass	Position		
	x_b (m)	y_b (m)	z_b (m)
400	0.400	0.000	0.000
400	-0.400	0.000	0.000
500	0.000	0.500	0.000
500	0.000	-0.500	0.000
550	0.000	0.000	1.400
550	0.000	0.000	-1.400

Table 2 – Solar panels of the satellite

Parameter	Values
Number of solar panels	2
Each solar panel's dimension	12 m × 2.4 m × 0.03 m
Number of elements in each solar panel	16
Dimension of each element	1.50 m × 1.20 m × 0.03 m
Poisson ratio, ν	0.3
Mass density, ρ	120 kg/m^3
Young's modulus of elasticity, E	0.6×10^8 N/m^2
Distance between O_b and panel's root	1.80 m
Offset angle of solar panels, δ	30°

At initial condition, the satellite is in an undeform state, while under normal operating conditions according to the satellite design the main body fixed reference frame coincides with the orbital reference frame and inertial reference frame. The orbital reference frame, F_o rotates about the inertial reference frame, F_i with a constant angular velocity,

$$\omega_o = -\omega_o \mathbf{j}_i \tag{5}$$

In Equation (5), $\mathbf{j}_i$ is the unit vector in the direction of the Y_i axis and $\omega_o = 7.29 \times 10^{-5}$ rad/s. It means that the satellite orbits the earth once a sidereal day. Using the parameters of the main body and solar panels as listed in Tables 1 and 2, and setting the constraint that the base of the solar panels do not deflect due to relatively rigid reinforcing structures, the satellite will have 144 natural frequencies of vibration.

The first and second natural frequencies of vibrations are $\omega_1 = 0.3354$ rad/s and $\omega_2 = 1.082$ rad/s, respectively. These two natural frequencies are the oscillation frequencies for the coupling roll and yaw motions.

If there is no disturbance, the satellite in this research operates in orbit with roll, pitch and yaw angles, all 0°. Then in the simulation the satellite is supposed to be at rest but has an attitude error, where the attitude angle is initially -3° in roll, -1° in pitch and 2° in yaw. Therefore it is necessary to do attitude correction where all attitude angles must be moved to 0°. For this attitude change, bang-bang torques are used, both in the roll, pitch and yaw directions. These torques are generated by thruster bursts. The torque here is 8 Nm, in both roll, pitch and yaw directions.

To make this desired maneuver, bang-bang torques in the direction of the roll T_{bx}, pitch T_{by} and yaw T_{bz} are required for 21.528 s, 4.744 s and 16.444 s, respectively. To correct the attitude in the fastest time then T_{bx}, T_{by} and T_{bz} are applied since $t = 0$ simultaneously. When the satellite experiences roll, pitch and yaw torques simultaneously from the initial time of simulation, the attitude angles and deflection of node 27 are shown in Figs. 3 and 4, respectively. Node 27 is the nodal point at the tip-edge of the solar panel at the positive Y_b axis direction. Seen in Fig. 3 that all angles of attitude have been successfully changed to the desired attitude.

At the end of the maneuver, as seen in Figs. 3 and 4, all attitude angles and structural deflection of node 27 have very large residual oscillations. Node 27 experienced out-of-plane vibrations with a very high amplitude of 1.46 meters. When compared with the length of the solar panel which is 12 m, the deflection is about 12%. Their oscillations predominantly occur in the vibration period of 18.73 seconds. This period of vibration corresponds to the first natural frequency of the satellite.

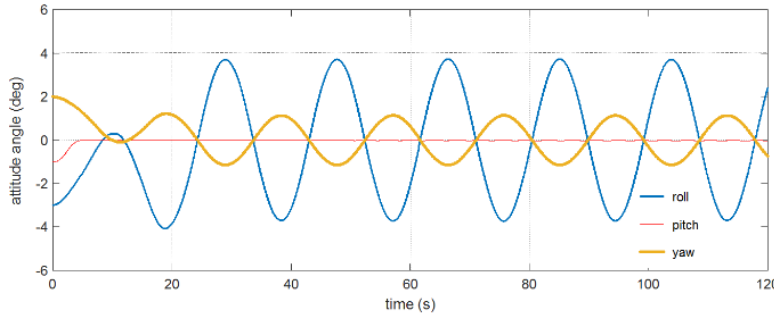

Fig. 3 – Time history of attitude angle displacement under the bang-bang torques

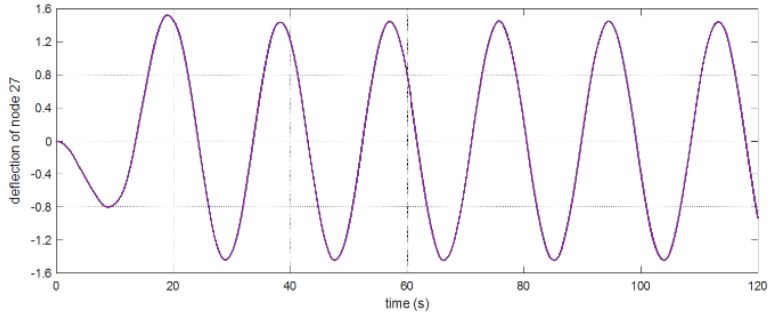

Fig. 4 – Time history of local vertical displacement of node 27 under the bang-bang torques

4. FUEL-EFFICIENT INPUT SHAPERS WITH TWO CONSTANT-AMPLITUDES

An appropriate torque input to drive the flexible satellite attitude to the desired attitude with negligible or non-existent residual vibration can be 'created'. This method is referred to as input shaping [29]. In this method, the time location and the applied input amplitude are planned and determined by simultaneously solving a number of constraint equations. In this paper, the control torque generated by the on-off thruster can have two constant amplitudes, i.e. T and 0.5 T. We selected two fuel-efficient type input shaping configurations in this rest-to-rest attitude maneuver. The input consists of two pulses in the positive direction and two pulses in the negative direction.

One we define as LHHL, while the other as HLLH. In both of these definitions, L denotes an input with a 'low' amplitude, while H denotes an input with a 'high' amplitude. So for example, the LHHL input whose configuration is shown in Fig. 5 would consist of four torque pulses as a result of gas emission: a first low-amplitude torque pulse, a second high-amplitude, a third high-amplitude, and a fourth low-amplitude torque pulse. Why are the third and fourth torque pulses in the opposite direction to the first and second? This is done to create a rest-to-rest maneuver. The first and second torque pulses will produce a positive angular acceleration - in the sense that they are in the direction of the desired angular displacement - meaning they will produce a positive angular velocity at the end of the second torque pulse. For the final state to stop, this angular velocity must be zeroed again at the end of the fourth torque pulse. The implementation is of course by providing angular deceleration, or in other words providing angular acceleration in the negative direction. The same applies to another definition, namely HLLH whose configuration is shown in Fig. 6.

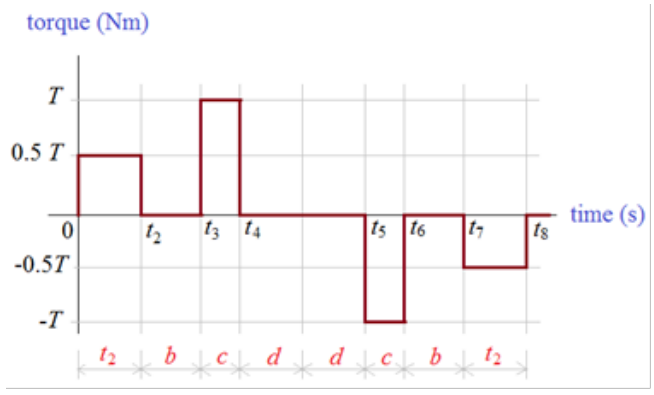

Fig. 5 – Fuel-efficient LHHL torque input configuration

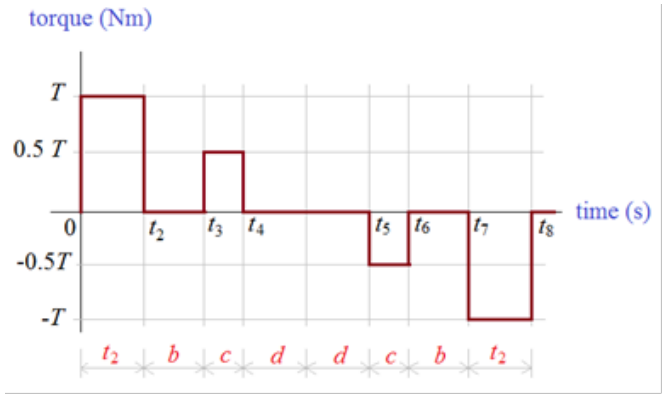

Fig. 6 – Fuel-efficient HLLH torque input configuration

4.1 Fuel-efficient LHHL input shaper

For the first input configuration as shown in Fig. 5, LHHL, the alternative signal pulse sequence can be expressed as the convolution of the step input with the input shaper in the form of

$$\begin{bmatrix} A_i \\ t_i \end{bmatrix} = \begin{bmatrix} 0.5 & -0.5 & 1 & -1 & -1 & 1 & -0.5 & 0.5 \\ t_1 & t_2 & t_3 & t_4 & t_5 & t_6 & t_7 & t_8 \end{bmatrix} \tag{6}$$

For a rest-to-rest maneuver, attitude angle velocity in Equation (3) must be zero. To guarantee this condition, it was selected a symmetrical condition for time location of impulses with $t_1 = 0$. For any arbitrary $t_2 > t_1$,

$$\begin{gathered} t_3 = t_2 + b \\ t_4 = t_3 + c = t_2 + b + c \\ t_5 = t_4 + 2d = t_2 + b + c + 2d \\ t_6 = t_5 + c = t_2 + b + 2c + 2d \\ t_7 = t_6 + b = t_2 + 2b + 2c + 2d \\ t_8 = t_7 + t_2 = 2t_2 + 2b + 2c + 2d \end{gathered} \tag{7}$$

The a, b, c and d are positive variables those must produce

$$a\left\{\frac{1}{2}{t_2}^2 + t_2 b + t_2 c + c^2 + (t_2 + 2c)d\right\} = \Theta_{des} \tag{8}$$

where Θ_{des} is the desired angular rotation which can be the desired roll, pitch or yaw angle displacement. The variable a is the angular acceleration, i.e. the acceleration component in Equation (2).

The next constraint is to limit the residual vibration at a certain natural frequency ω to a desired value. Percentage of residual vibration of the input Equation (6) to the bang-bang input that produces the desired maneuver can be written as follows:

$$V(\omega) = \sqrt{\frac{[\sum A_i \, sin(\omega t_i)]^2 + [\sum A_i \, cos(\omega t_i)]^2}{\left[\sum A_{bbj} \, sin(\omega t_{bbj})\right]^2 + \left[\sum A_{bbj} \, cos(\omega t_{bbj})\right]^2}} \times 100\% \tag{9}$$

where A_{bbj} and t_{bbj} express the input shaper for the bang-bang in the following expression

$$\begin{bmatrix} A_{bbj} \\ t_{bbj} \end{bmatrix} = \begin{bmatrix} 1 & -2 & 1 \\ t_1 & t_2 & t_3 \end{bmatrix} \tag{10}$$

Equation (9) can be made as many times as needed. For example, the equation is made for residual vibrations at the first, second, third natural frequencies and so on. Using the above constraints, a large number solutions for t_i (i = 1, 2, …, 8) can be resulted. If we want to maneuver the satellite as soon as possible, then we must select the smallest value of t_8,

$$\text{minimize}(t_8) \tag{11}$$

It should be noted that Equations (6)-(11) are defined to make the angular displacement in the positive direction. If it turns out that the desired angular displacement is in the negative direction, then we only need to multiply Equations (6) and (10) by -1. Also, Equations (6) and (10) are defined to give a maximum input torque of 1 Nm. To convert to the actual torque input generated by the satellite, these equations must be multiplied by T.

4.2 Fuel-efficient HLLH input shaper

In contrast to the first configuration, the series of alternative-signal pulses in HLLH shown in Fig. 6 can be expressed as the convolution of the step input with the input shaping in the form of

$$\begin{bmatrix} A_i \\ t_i \end{bmatrix} = \begin{bmatrix} 1 & -1 & 0.5 & -0.5 & -0.5 & 0.5 & -1 & 1 \\ t_1 & t_2 & t_3 & t_4 & t_5 & t_6 & t_7 & t_8 \end{bmatrix} \tag{12}$$

For the selection of t_i (i = 1, 2, …, 8) as written in Equation (7), the values of a, b, c and d must be determined in order to produce the attitude angular displacement in accordance with the desired value.

$$a\left\{{t_2}^2 + 2t_2 b + (2t_2 + \frac{1}{2}c)c + 2(t_2 + \frac{1}{2}c)d\right\} = \Theta_{des} \tag{13}$$

Finally, Equations (9)-(11) are also used as the constraint equations for HLLH configuration. The note in the final paragraph of Section 4.1 above also applies to Equation (12).

5. SIMULATION AND DISCUSSIONS

To demonstrate the usefulness and power of shaped HLLH and LHHL inputs in this paper, simulations with initial and final conditions as performed in Section 3 will be repeated. In that section we find the fact that the residual oscillation of the pitch angle is very small. Therefore the input shaping method need not be applied to the pitch torque. The bang-bang pitch torque

can be directly applied to the satellite without modification. The input shaping technique is applied to roll and yaw torques to dampen residual vibrations after attitude maneuvers.

Ideally, vibrations at all natural frequencies need to be dampened so that there are no residual vibrations anymore. However, there may not be a solution torque input that can completely dampen all vibrations.

Whereas vibrations at high frequencies usually occur with a fairly small amplitude and do not interfere with the satellite's accuracy in pointing to the earth. In this simulation it is assumed that only vibrations at the two natural frequencies produce residual structural vibrations which are quite disturbing.

Therefore, the constraints in Equation (9) are only applied to the first two natural frequencies for roll and yaw satellite oscillations.

The residual vibration at $\omega = 0.3354$ rad/s is so large as simulated in Section 3 that it needs to be completely suppressed.

It may be very unlikely to get a value of 0% in the residual vibration calculation. We believe that an error tolerance of 0.001% is quite acceptable for a residual vibration value equal to zero, so in this case we put $V(0.3354) < 0.001\%$.

The residual vibration at $\omega = 1.082$ rad/s is assumed to be quite large and needs to be suppressed to a sufficiently small value, so we place $V(1.082) < 1\%$. The resulting shortest inputs are listed in Table 3.

Table 3 – Time location of impulses to shape the roll and yaw torque inputs

	t_1 (s)	t_2 (s)	t_3 (s)	t_4 (s)	t_5 (s)	t_6 (s)	t_7 (s)	t_8 (s)
Roll, LHHL	0	1.240	3.270	8.730	21.229	26.689	28.719	29.959
Yaw, LHHL	0	1.630	2.360	5.140	19.834	22.614	23.344	24.974
Roll, HLLH	0	6.040	7.880	8.220	16.753	17.093	18.933	24.973
Yaw, HLLH	0	1.720	2.420	6.230	17.780	21.590	22.290	24.010

Using the yaw and roll torque inputs of Table 3 coupled with the bang-bang pitch torque input, the attitude maneuvers of the flexible satellite are computationally simulated. The initial condition of the satellite is as same as the simulation using bang-bang torques input in Section 3. The satellite is at rest condition in the undeform state.

The attitude of the main body of the satellite is -3° in roll, -1° in pitch and 2° in yaw. It must be maneuvered into 0° attitude angles.

The magnitude of torque T in Figs. 5 and 6 is selected to be 8 Nm. The LHHL input gives the attitude angle and solar panel's tip deflection responses as shown in Figs. 7 and 8, respectively.

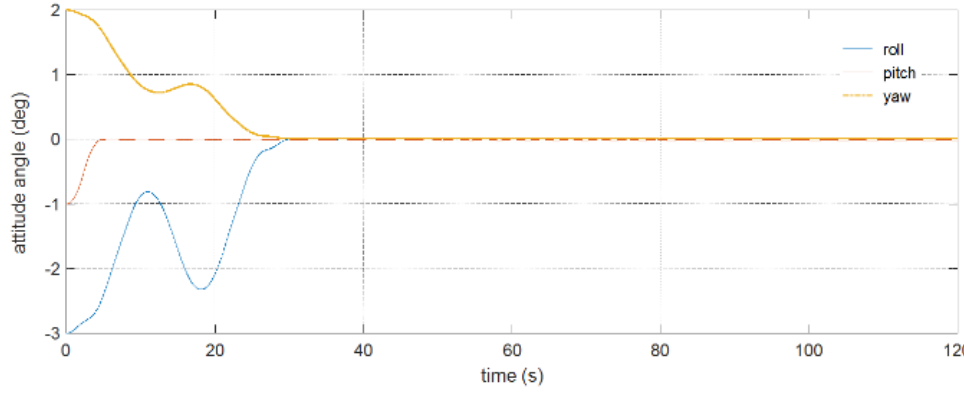

Fig. 7 – Time history of attitude angle displacement under the fuel-efficient LHHL roll and yaw torques

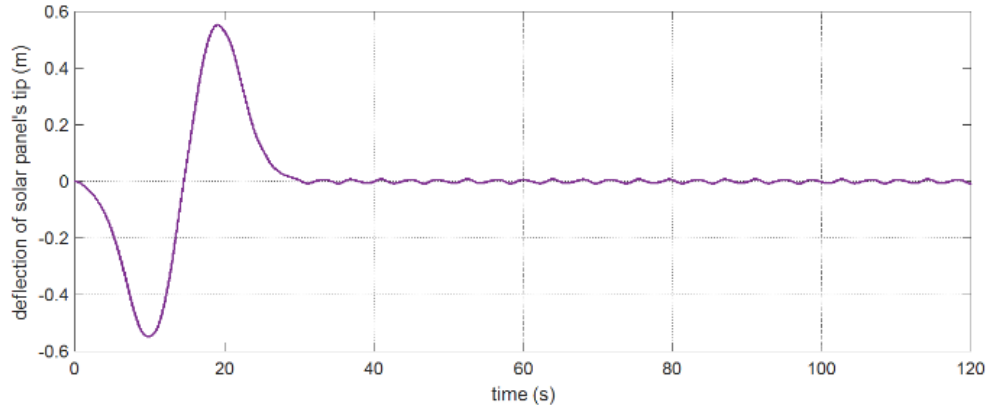

Fig. 8 – Time history of local vertical displacement of node 27 under the fuel-efficient LHHL roll and yaw torques

It can be seen in Figure 7 that all attitude angles can be changed to 0° with very small residual oscillations after the maneuver. The residual vibration at node 27 is quite small as shown in Figure 8.

The results in the figures have proven that our assumption that it is only necessary to dampen vibrations at the first two natural frequencies to produce good attitude accuracy on the satellites we simulate is correct.

The LHHL input for this maneuver has a roll torque in the form of pulses with an amplitude of 4 Nm, either in the positive or negative direction, along $(t_{2,\phi} - t_{1,\phi}) + (t_{8,\phi} - t_{7,\phi}) =$ 2,480 s; while the pulses have an amplitude of 8 Nm for $(t_{4,\phi} - t_{3,\phi}) + (t_{6,\phi} - t_{5,\phi}) = 10.920$ seconds. In the yaw direction, a torque input with the pulses of a 4-Nm amplitude is required for $(t_{2,\psi} - t_{1,\psi}) + (t_{8,\psi} - t_{7,\psi}) = 3.260$ seconds and pulses with an amplitude of 8 Nm is required for $(t_{4,\psi} - t_{3,\psi}) + (t_{6,\psi} - t_{5,\psi}) = 5.560$ seconds.

If thruster fuel is needed when the torque pulse is on and not needed when the pulse is off, then the control time length using fuel is 13.400 seconds for roll and 8.820 seconds for yaw. The maximum deflection of node 27 of 0.55 m occurs at about $t = 9.98$ s during the transient response, as shown in Fig. 8.

Figs. 9 and 10 show the responses of the satellite attitude angles and the deflection of the solar panel tip, namely node 27, respectively.

We can see in Fig. 9 that the satellite attitude error at the beginning of the simulation was successfully corrected at the end of the maneuver. Residual oscillations of the attitude angles of the satellite are also very well suppressed. The residual vibration at node 27 was also suppressed well as shown in Fig. 10.

The HLLH input for this maneuver has a torque requiring fuel when pulses of amplitude 8 Nm on from t_1–t_2 and t_7–t_8, while from t_3–t_4 and t_5–t_6 the torque pulses with an amplitude of 4 Nm is required.

Thruster is off at t_2–t_3, t_4–t_5 and t_6–t_7 so that during these intervals it does not require fuel. The durations of 8 Nm and 4 Nm fueling pulses of the HLLH roll input are 12.080 s and 0.680 s, respectively; while for the yaw input are 3.440 s in 8 Nm and 7.620 s in 4 Nm.

The total fueling durations for the roll and yaw inputs are 12.760 s and 11.060 s, respectively. Fig. 10 shows that around 0.62-m transient deflection of node 27 at about $t = 7.84$ s will be generated.

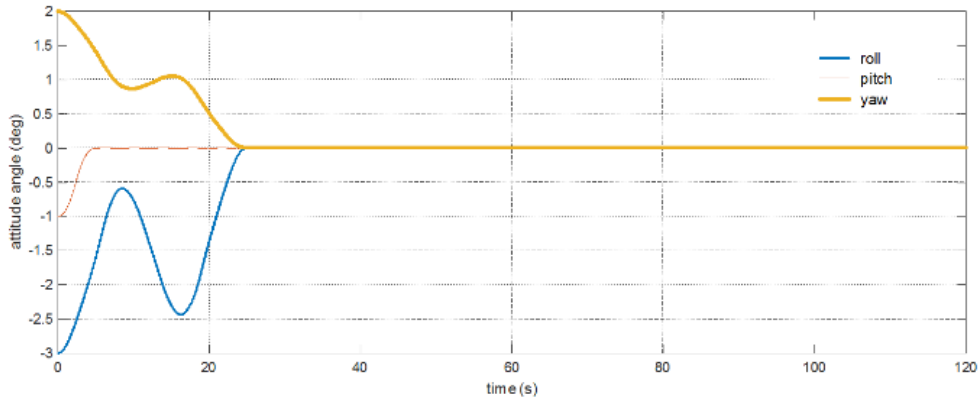

Fig. 9 – Time history of attitude angle displacement under the fuel-efficient HLLH roll and yaw torques

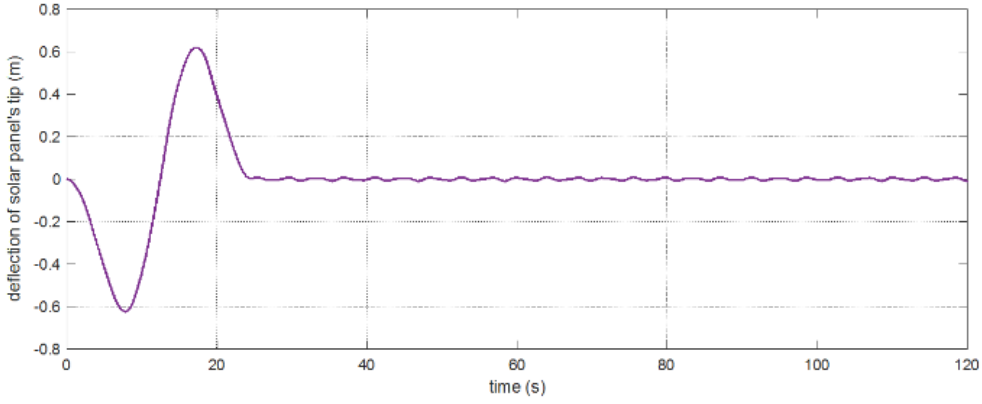

Fig. 10 – Time history of local vertical displacement of node 27 under the fuel-efficient HLLH roll and yaw torques

The maneuver using the fuel-efficient LHHL input shaper is completed in 29.959 seconds, while using the HLLH takes 24.973 seconds. Thus, using the HLLH input shaper will route the satellite 17% faster than LHHL.

The fuel consumption period for the LHHL input shaper is 13,400 s in roll and 8,820 s in yaw, while for HLLH it is 12,760 s in roll and 11,060 s in yaw. So, in terms of the duration of fuel use, we cannot specifically conclude here.

When viewed from the variable (torque × duration), for roll motion with LHHL it takes (4 Nm × 2,480 s) + (8 Nm × 10,920 s) = 97,280 Nms and for yaw it takes (4 Nm × 3,260 s) + (8 Nm × 5.560 s) = 57.520 Nms, whereas HLLH requires (8 Nm × 12.080 s) + (4 Nm × 0.680 s) = 99.360 Nms in coils and (8 Nm × 3.44 s) + (4 Nm 7.62 s) = 58 Nms.

This means that in terms of Nms LHHL requires a smaller value than HLLH. If the propulsion muzzle that produces either T or 0.5 T of torque is the same, then 0.5 T means that it requires only half the propulsion force of T.

Thus the magnitude of Nms is proportional to the amount of fuel consumption. So the use of the LHHL input shaper will be more fuel efficient than the HLLH.

Lastly, in terms of maximum transient deflection of the solar panel tip, LHHL produces less deflection than HLLH. The HLLH deflection will be 13% greater than the result with LHHL.

6. CONCLUSIONS

Two configurations of fuel-efficient input formation in two constant amplitudes for correcting the satellite attitude with two flexible solar panels are studied in this paper. The location of the impulse timing to form the input is chosen to be symmetrical. The first configuration –LHHL– starts with a smaller constant amplitude, which is 4 Nm, while the second configuration –HLLH– starts with a higher constant amplitude, which is 8 Nm. Attention is paid to the time required for the satellite maneuvering process and the induced deflection of the solar panels during the transient response. The results show that for the desired roll, pitch and yaw angular displacements of 3°, 2° and -2°, respectively, we need to sufficiently dampen the vibrations at the two lowest natural frequencies. The input shaping the HLLH is capable of changing the satellite's attitude 17% faster than the LHHL. In terms of fuel consumption, LHHL input is more efficient than HLLH. Also, in terms of structural deflection during the transient response, the input shaper with the LHHL configuration provides a structural deflection that is 13% smaller than the HLLH input shaper. This means that in terms of producing a small structural deflection, the LHHL input shaper has better performance.

REFERENCES

[1] https://spaceflight101.com/spacecraft/intelsat-30-dla-1/, [Accessed: 22 August 2022].
[2] https://www.researchgate.net/publication/316734562_Satellite_space_systems_-_electrical_power_systems. [Accessed: 22 August 2022].
[3] https://spaceflight101.com/spacecraft/wgs-wideband-global-satcom/. [Accessed: 22 August 2022].
[4] S. Parman, H. Koguchi, Controlling the attitude maneuvers of flexible spacecraft by using time-optimal/fuel-efficient shaped inputs, *Journal of Sound and Vibration*, vol. **221**, iss. 4, pp. 545-565, 8 April 1999, https://doi.org/10.1006/jsvi.1998.2045
[5] S. Parman, H. Koguchi, Rest-to-Rest Attitude Maneuvers and Residual Vibration Reduction of a Finite Element Model of Flexible Satellite by Using Input Shaper, *Shock and Vibration*, vol. 6, iss. 1, pp. 11-27, 1999, https://doi.org/10.1155/1999/702162
[6] S. Parman, Controlling attitude maneuvers of flexible spacecraft based on nonlinear model using combined feedback-feedforward constant-amplitude inputs, *2013 10th IEEE International Conference on Control and Automation (ICCA)*, pp. 1584-1591, 2013, doi: 10.1109/ICCA.2013.6565098
[7] S. Parman, T. H. Go, Tuwoso, Two constant amplitude pulses' input shaper to maneuver an attitude of precise-oriented flexible spacecraft, *Journal of Sound and Vibration*, vol. **465**, article 115011, 20 January 2020, https://doi.org/10.1016/j.jsv.2019.115011
[8] S. Parman, H. Koguchi, Rest-to-rest attitude maneuvers of a satelite with flexible solar panels by using input shapers, *Computer Assisted Mechanics and Engineering Sciences*, vol. **5**, no. 4, pp. 421-441, 1998.
[9] S. Parman, H. Koguchi, Fuel-efficient attitude maneuvers of flexible spacecraft with residual vibration reduction into an expected level, *Computer Assisted Mechanics and Engineering Sciences*, vol. 7, no. 1, pp. 11-21, 2000.
[10] W. Singhose, S. Derezinski, N. Singer, Extra-insensitive input shapers for controlling flexible spacecraft, *Journal of Guidance, Control and Dynamics*, vol. **19**, no. 2, pp. 385-391, March-April 1996, https://doi.org/10.2514/3.21630
[11] W. Singhose, L. Pao, A comparison of input shaping and time-optimal flexible-body control, *Contr. Eng. Pract*., vol. **5**, iss. 4, pp. 459-467, April 1997, https://doi.org/10.1016/S0967-0661(97)00025-7
[12] X. Zhang, Q. Zong, L. Dou, B. Tian, W. Liu, Finite-time attitude maneuvering and vibration suppression of flexible spacecraft, *Journal of the Franklin Institute*, vol. **357**, iss. 16, pp. 11604-11628, November 2020, https://doi.org/10.1016/j.jfranklin.2019.09.003
[13] J. Wang, J. Wu, J. Zou, Flexible spacecraft attitude maneuver planning based on variable amplitudes input shaping method, *Guofang Keji Daxue Xuebao/Journal of National University of Defense Technology*, vol. **44**, no. 1, pp. 68 – 76, 2022, https://doi.org/10.11887/j.cn.202201011
[14] Y. Du, C. Wang, Y. Zhou, J. Lu, Vibration Control for Flexible Spacecraft Using Multi-Impulse Robust Input Shaper and Optimal Control Method, *Advances in Applied Mathematics and Mechanics*, vol. **12**, no. 3, pp. 797-814, 2020, https://doi.org/10.4208/aamm.OA-2019-0055

[15] W. Zhu, Q. Zong, X. Zhang, W. Liu, *Disturbance observer-based multivariable finite-time attitude tracking for flexible spacecraft*, 2020 39th Chinese Control Conference (CCC), pp. 1772-1777, 2020, https://doi.org/10.23919/CCC50068.2020.9188575

[16] C. Nieto-Peroy, G. Palmerini, É. J. de Oliveira, P. Gasbarri, M. Sabatini, M. Milz, Simulation of Spacecraft Formation Maneuvers by means of Floating Platforms, *2021 IEEE Aerospace Conference (50100)*, pp. 1-10, 2021, https://doi.org/10.1109/AERO50100.2021.9438537

[17] X. Liu, L. Lv, G. Cai, Hybrid control of a satellite with membrane antenna considering nonlinear vibration, *Aerospace Science and Technology*, vol. **117**, 106962, 2021, https://doi.org/10.1016/j.ast.2021.106962

[18] Y-G. Sung, C-L. Kim, Deflection Reduction Shaping Commands with Asymmetric First-Order Actuators, *Appl. Sci*., vol. **9**, no. 19, 3982, 2019, https://doi.org/10.3390/app9193982

[19] W. E. Singhose, A. K. Banerjee, W. P. Seering, Slewing flexible spacecraft with deflection-limiting input shaping, *J. Guid. Control Dyn*., vol. **20**, no. 2, pp. 291-298, 1997, https://doi.org/10.2514/2.4036

[20] Y-G. Sung, W. E. Singhose, Limited-state commands for systems with two flexible modes, *Mechatronics*, vol. **19**, iss. 5, pp. 780-787, August 2009, https://doi.org/10.1016/j.mechatronics.2009.03.001

[21] A. Alshaya and K. Alhazza, Smooth and robust multi-mode shaped commands, *Mechanical Systems and Signal Processing*, vol. **168**, 108658, April 2022, https://doi.org/10.1016/j.ymssp.2021.108658

[22] M.J. Maghsoudi, L. Ramli, S. Sudin, Z. Mohamed, A.R. Husain, H. Wahid, Improved unity magnitude input shaping scheme for sway control of an underactuated 3D overhead crane with hoisting, *Mechanical Systems and Signal Processing*, vol. **123**, pp. 466–482, 2019, https://doi.org/10.1016/j.ymssp.2018.12.056

[23] M. Khairudin, S. P. Herlambang, Y. Sigit, A. Andik, T. Herawan, Z. Mohamed, A. Shah and M. N. A. Azman, Modelling and State Variable Feedback Control with Proportional Action of a One-Link Flexible Manipulator Incorporating Payload, *International Journal of Acoustics and Vibration*, vol. **26**, no. 1, pp. 9-17, 2021, https://doi.org/10.20855/ijav.2020.25.11489

[24] M. J. Robertson, Transient deflection performance measures for command shapers, *2008 American Control Conference*, pp. 3251-3256, 2008, https://doi.org/10.1109/ACC.2008.4586993

[25] S. Parman, Study on structural deflection of flexible satellite during attitude maneuver using fuel-efficient input shaper, *2016 SICE International Symposium on Control Systems (ISCS)*, pp. 1-6, 2016, https://doi.org/10.1109/SICEISCS.2016.7470156

[26] S. Parman, Maneuvering the attitude of precise-oriented flexible satellite using input shaper in small transient structural deflection, *2016 17th International Carpathian Control Conference (ICCC)*, pp. 552-557, 2016, https://doi.org/10.1109/CarpathianCC.2016.7501158..

[27] J. M. Raya-Armenta, N. Bazmohammadi, J.C. Vasquez, J.M. Guerrero, A short review of radiation-induced degradation of III–V photovoltaic cells for space applications, *Solar Energy Materials and Solar Cells*, vol. **233**, 111379, December 2021, https://doi.org/10.1016/j.solmat.2021.111379

[28] R. D. Robinett, G. G. Parker, Spacecraft Euler parameter tracking of large-angle maneuvers via sliding mode control, *Journal of Guidance, Control and Dynamics*, vol. **19**, no. 3, 1996, https://doi.org/10.2514/3.21677

[29] W. Singhose, K. Bohlke, W. P. Seering, Fuel-efficient pulse command profiles for flexible spacecraft, *Journal of Guidance, Control and Dynamics*, vol. **19**, no. 4, pp. 954-960, July 1996, https://doi.org/10.2514/3.21724